

# Magnetic Transformations in the Organic Conductor $\kappa$ -(BETS)<sub>2</sub>Mn[N(CN)<sub>2</sub>]<sub>3</sub> at the Metal-Insulator Transition

O. M. Vyaselev,<sup>1</sup> M. V. Kartsovnik,<sup>2</sup> W. Biberacher,<sup>2</sup> L. V. Zorina,<sup>1</sup> N. D. Kushch,<sup>3</sup> and E. B. Yagubskii<sup>3</sup>

<sup>1</sup>*Institute of Solid State Physics, Russian Academy of Sciences, Chernogolovka, Moscow region, 142432, Russia*

<sup>2</sup>*Walther-Meißner-Institut, Bayerische Akademie der Wissenschaften, Garching, Germany*

<sup>3</sup>*Institute of Problems of Chemical Physics, Russian Academy of Sciences, Chernogolovka, Moscow region, 142432, Russia*

(Dated: November 6, 2018)

A complex study of magnetic properties including dc magnetization, <sup>1</sup>H NMR and magnetic torque measurements has been performed for the organic conductor  $\kappa$ -(BETS)<sub>2</sub>Mn[N(CN)<sub>2</sub>]<sub>3</sub> which undergoes a metal-insulator transition at  $T_{MI} \approx 25$  K. NMR and the magnetization data indicate a transition in the manganese subsystem from paramagnetic to a frozen state at  $T_{MI}$ , which is, however, not a simple Néel type order. Further, a magnetic field induced transition resembling a spin flop has been detected in the torque measurements at temperatures below  $T_{MI}$ . This transition is most likely related to the spins of  $\pi$  electrons localized on the organic molecules BETS and coupled with the manganese  $3d$  spins via exchange interaction.

PACS numbers: 74.70.Kn, 71.30.+h, 71.27.+a, 75.30.-m, 75.30.Gw, 75.30.Cr, 76.60.Jx

## I. INTRODUCTION

Quasi-two-dimensional organic charge transfer complexes can be visualized as sheets of organic donor/acceptor molecules sandwiched between insulating anion/cation layers.<sup>1</sup> Conductivity in such materials is associated with organic layers. For years they have been in focus of extensive research activities because these high-purity materials with relatively simple Fermi surfaces offer rich pressure-temperature-field ( $P$ - $T$ - $B$ ) phase diagrams. As a result of the interplay between electron correlations, the electron-phonon interaction, the electron kinetic energy, and characteristics of the Fermi surface topology, the phase diagram can include metal-insulator (MI) and superconducting (SC) transitions as well as different kinds of charge and spin ordering: charge and spin density waves, long-range antiferromagnetic (AF) order, spin glass etc.<sup>1,2</sup> Synthesis of radical cation salts of organic  $\pi$ -donors with paramagnetic metal complex anions<sup>3-7</sup> has added a new dimension to the physics of organic conductors due to the implications of the interaction between the conduction electrons of the  $\pi$  band with localized  $d$  electrons. For example, interaction between localized spins in insulating magnetic layers and itinerant spins in conducting organic layers was found to lead to new fascinating phenomena such as field-induced superconductivity observed in  $\lambda$ -(BETS)<sub>2</sub>FeCl<sub>4</sub><sup>8</sup> and  $\kappa$ -(BETS)<sub>2</sub>FeBr<sub>4</sub>,<sup>9</sup> where BETS stands for C<sub>10</sub>S<sub>4</sub>Se<sub>4</sub>H<sub>8</sub>, bis(ethylenedithio)tetraselenafulvalene.

The recently synthesized layered conductor  $\kappa$ -(BETS)<sub>2</sub>Mn[N(CN)<sub>2</sub>]<sub>3</sub><sup>10</sup> is expected to give a thrilling combination of potentially non-trivial magnetic properties arising from the nearly triangular network of Mn<sup>2+</sup> ions in the anion layer, with strong electron correlations characteristic of the narrow half-filled conducting band of organic layers. At ambient pressure, this material undergoes a MI transition at  $T_{MI} \simeq 25$  K, which however

can be suppressed by applying a relatively low external pressure, giving way to a superconducting state with maximum  $T_c = 5.75$  K at  $P = (0.6 - 1.0)$  kbar.<sup>11</sup> Resistivity measurements combined with X-ray studies and electronic band structure calculations<sup>11</sup> have suggested the electronic ground state to be a Mott insulator. However, the question about the role of the interaction between itinerant spins in the donor layers and localized spins of Mn<sup>2+</sup> in the formation of the insulating ground state is still open. For example, it was believed that in  $\lambda$ -(BETS)<sub>2</sub>FeCl<sub>4</sub> where the MI and the AF transitions coexist,<sup>12</sup> the magnetic ordering in Fe<sup>3+</sup> subsystem leads to localization of  $\pi$ -electrons of BETS.<sup>13</sup> However, recent specific heat<sup>14</sup> and Mössbauer<sup>15</sup> studies have casted doubt on this viewpoint, suggesting that the magnetic order only exists among the localized  $\pi$ -electrons while the Fe<sup>3+</sup> moments stay paramagnetic.

To clarify the issue of the  $\pi$ - $d$  interaction, its influence on the phase diagram of  $\kappa$ -(BETS)<sub>2</sub>Mn[N(CN)<sub>2</sub>]<sub>3</sub>, and to understand the driving force of the MI transition, we have studied its magnetic properties revealed by dc magnetization, magnetic torque, and NMR measurements. In this paper we report results of this investigation, arguing for a magnetic transition caused apparently by the MI transition.

## II. EXPERIMENTAL

The crystal structure of  $\kappa$ -(BETS)<sub>2</sub>Mn[N(CN)<sub>2</sub>]<sub>3</sub> is monoclinic with the space group  $P2_1/c$  and the lattice constants at 90 K  $a=19.453(5)\text{\AA}$ ,  $b=8.381(5)\text{\AA}$ ,  $c=11.891(5)\text{\AA}$ ,  $\beta=92.784(5)^\circ$ , and  $V=1936.37\text{\AA}^3$ , with two formula units per unit cell<sup>10</sup>. The conducting layers are formed by BETS dimers in the ( $bc$ ) plane and sandwiched between the polymeric Mn[N(CN)<sub>2</sub>]<sub>3</sub> anion layers in the  $a$  direction. The crystal growth procedure and details of the structure have been described elsewhere.<sup>10,11</sup>

The samples were thin-plate single crystals of  $\sim 1 \times$

$0.5 \times 0.1 \text{ mm}^3$  size, with the largest dimension along the conducting BETS layers [crystallographic ( $bc$ ) plane]. Crystallographic orientations for each crystal were X-ray defined. The dc magnetization of a  $90 \mu\text{g}$  sample was measured using Quantum Design MPMS-XL SQUID magnetometer in fields from 1 to 70 kOe. The sample was fixed between two  $6 \times 6 \times 1 \text{ mm}^3$   $\text{SrTiO}_3$  (STO) plates for  $H \perp (bc)$  and on a  $5 \times 5 \times 0.2 \text{ mm}^3$  Si plate for  $H \parallel (bc)$  measurements. Magnetic moments of the substrates were measured separately for reference.  $^1\text{H}$  NMR was measured using Bruker MSL-300 spectrometer in fields 14 and 70 kOe on a  $\sim 100 \mu\text{g}$  crystal attached to a quartz holder with a touch of silicon grease. The empty holder with the grease gave no  $^1\text{H}$  NMR signal on the scale of the signal from the sample. Magnetic torque from a  $40 \mu\text{g}$  sample was measured in fields up to 150 kOe with a home-made cantilever beam torque meter described in Ref. 16. The cantilever was made of as-rolled beryllium-copper foil  $50 \mu\text{m}$  thick.

### III. RESULTS AND DISCUSSION

#### A. dc magnetization

In agreement with the earlier report,<sup>10</sup> the measured magnetic moment of the sample grows with diminishing temperature obeying the Curie law down to  $T_{MI} \simeq 25 \text{ K}$ : the sample magnetization per mole,  $M$ , is quite precisely described as  $M = \chi_{CW}H$ , where  $\chi_{CW} = C_m/(T - \theta)$  is the Curie-Weiss susceptibility. With the Curie constant  $C_m = 4.38 \text{ cm}^3\text{K/mol}$  calculated for the Landé factor  $g = 2$  and the total angular momentum  $J = 5/2$ , the fits to the experimental data give  $\theta = -5.9, -4.6,$  and  $-4.9 \text{ K}$  for the field directions along the  $a^*$  [ $\perp (bc)$ ],  $b$ , and  $c$  axes, respectively. Figure 1 shows temperature dependences of the inverse susceptibility,  $\chi^{-1} = H/M$ , as well as  $\chi/\chi_{CW} - 1$ , the relative deviation of  $\chi$  from the Curie-Weiss value, for the field  $H = 1 \text{ kOe}$  applied along the  $a^*$ ,  $b$ , and  $c$  directions. One can see that at  $T > 25 \text{ K}$  the susceptibility is essentially isotropic, following accurately the Curie-Weiss law. This denotes that the system magnetization in this region is dominated by localized moments of  $\text{Mn}^{2+}$  in high-spin state ( $L = 0, S = 5/2$ ) with AF interactions, as follows from the negative sign of  $\theta$ .

As the system enters the insulating state below 25 K, the susceptibility turns down from  $\chi_{CW}$ . Hardly visible in the  $\chi^{-1}(T)$  plot, this deviation is clearly seen in the  $T$ -dependence of  $\chi/\chi_{CW} - 1$ , Fig.1. The absolute value of the drop of  $\chi$  from  $\chi_{CW}$  at 2 K is  $0.9 - 1.8 \times 10^{-1} \text{ cm}^3/\text{mol}$ , depending on the field direction, which is huge compared to the usual value ( $\leq 10^{-3} \text{ cm}^3/\text{mol}$ ) of the conduction electron spin susceptibility known for akin conducting non-magnetic organic compounds. Therefore the change of the magnetization behavior below the MI transition temperature should be attributed to a magnetic transformation in the  $\text{Mn}^{2+}$  network.

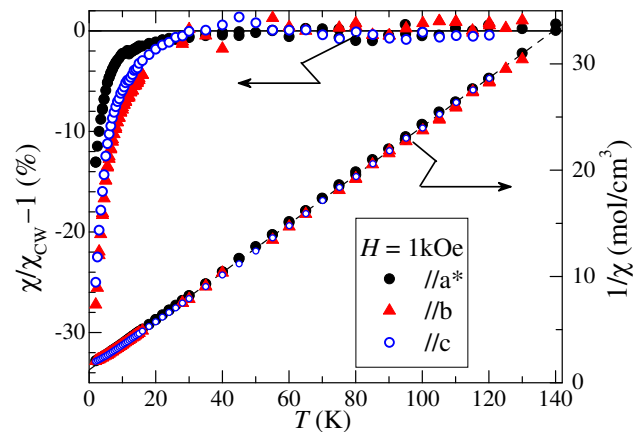


FIG. 1: (Color online) Temperature dependence of the inverse susceptibility,  $\chi^{-1} = H/M$  (right scale) and the relative deviation of  $\chi$  from the Curie-Weiss value (left scale) at a field of 1 kOe parallel to the  $a^*$ ,  $b$ , and  $c$ -axes.

Another evidence for this can be found in the field dependences of the magnetization. Within the molecular field theory, the exchange interaction between the localized moments is modeled as an additional magnetic field component  $H' = \lambda M$ , where  $\lambda$  is related to the Curie-Weiss temperature  $\theta$  as  $\lambda = C_m/\theta$ . The magnetization,  $M$ , in the paramagnetic state is then expressed in terms of  $(B_{eff}/T)$ , where the effective field  $B_{eff} = H + \lambda M$ .

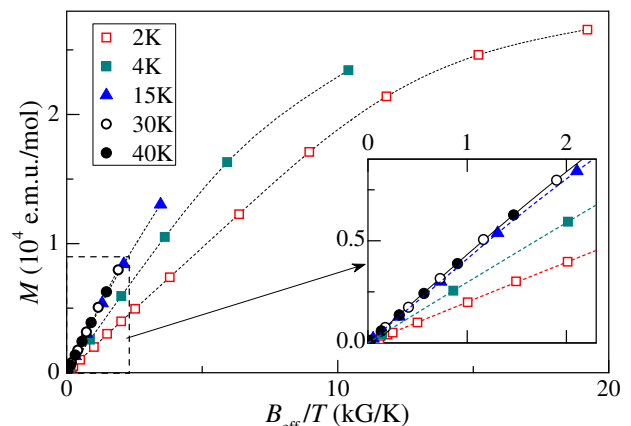


FIG. 2: (Color online)  $c$ -axis magnetization versus  $B_{eff}/T = (H + \lambda M)/T$  for several temperatures above and below the MI transition, with  $\lambda = -0.9$  corresponding to  $\theta = -4.9 \text{ K}$  obtained from the  $T$ -dependences of the magnetization. The inset is a close-up to demonstrate the universality of the plot for  $T > T_{MI}$ . Dashed lines are guides to the eye.

Fig. 2 demonstrates the  $c$ -axis magnetization plotted in function of  $B_{eff}/T = (H + \lambda M)/T$ , with  $\lambda = -0.9$  corresponding to  $\theta = -4.9 \text{ K}$  obtained from the  $T$ -dependences of the magnetization as described above. The same qualitative behavior has been obtained for the field applied along the  $a^*$ - and  $b$ -axes. At temperatures above 25 K, the magnetization is a universal function of

( $B_{eff}/T$ ), as is more clearly seen in the inset in Fig. 2, which is consistent with the paramagnetic state of AF-interacting  $Mn^{2+}$  ions. At lower temperature the magnetization declines from the common high- $T$  behavior, falling off more rapidly with diminishing temperature. This suggests that the state of the  $Mn^{2+}$  spin system below  $T_{MI}$  is no more paramagnetic.

### B. $^1H$ NMR

The title compound includes 8 inequivalent hydrogen sites which belong to the ethylene groups, located at the terminals of BETS molecules. Our study of the behavior of  $^1H$  NMR spectrum with rotating the magnetic field in the ( $ac$ ) plane at  $T = 74$  K has revealed 8 respective resonance peaks.<sup>17</sup> The angular dependence of each peak is *quantitatively* reproduced by a straightforward calculation of the dipolar field from the  $3d$   $Mn^{2+}$  ion electron spin moments ( $S = 5/2, g = 2$ ) (a detailed analysis of the  $^1H$  NMR data will be published separately). Furthermore, the proton NMR peak positions for  $H \parallel a^*$  at temperatures from 4 to 150 K are linear in dc magnetization for the same temperatures. This infers that protons probe the dipolar field induced by  $Mn^{2+}$  ions at hydrogen sites.

The inset in Figure 3 shows the NMR spectra measured at different temperatures in 14 kOe field applied along  $a^*$  direction. At this orientation, only 5 resonance lines are resolved due to overlapping of some of the peaks. To be more specific, the leftmost and the two rightmost peaks (at  $T \geq 20$  K) are from the individual hydrogen sites, while the central peak and the one next to the left are, respectively, three and two superimposed individual peaks.

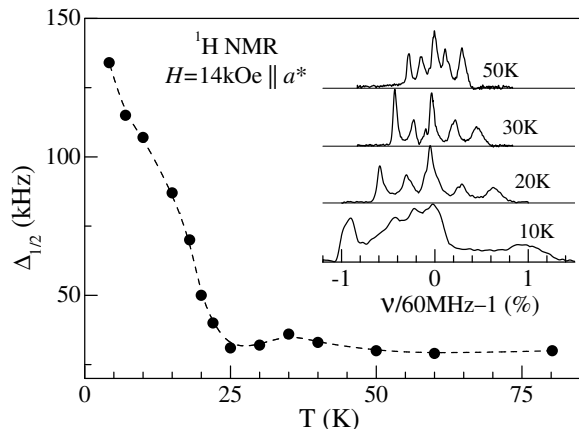


FIG. 3: Temperature dependence of the linewidth of the leftmost peak in the  $^1H$  NMR spectrum obtained at  $H = 14$  kOe parallel to  $a^*$ . Inset: NMR spectra at the same field orientation, at different temperatures.

As can be seen in the inset in Fig. 3, the  $^1H$  spectrum maintains its shape down to  $\sim 20$  K. At lower temper-

ature the peaks broaden rapidly, which is most noticeable on the right-hand side of the spectrum. In fact, below 10 K the right-hand side becomes a featureless pedestal spreading to several MHz up in frequency. The main panel of Fig. 3 shows the temperature dependence of the leftmost peak width measured at half height,  $\Delta_{1/2}$ . Rather flat above 25 K,  $\Delta_{1/2}$  increases sharply below this temperature.

One of the sources for the line broadening in the  $H \parallel a^*$  experiment could be a  $b$ -axis component of the internal field,  $H_b$ ,<sup>17</sup> which possibly exists if  $a^*$  is not a principal magnetic axis of the anisotropic material. However, the estimate of  $H_b$  using the measured dc magnetization,  $M_a = 9.65$  G, for  $H = 14$  kOe at 4.2 K, and the  $c$ -axis magnetic torque measurements addressed in the next section, give  $H_b < 0.2$  G which is negligible.

Therefore the increase of the linewidth below 25 K is due to enhancement of the scatter of the static local field induced by the electronic spin of  $Mn^{2+}$  at hydrogen sites. Assuming that the crystal structure is intact, this points to the appearance of manganese sites with different projections of the magnetic moment on the external field direction, i.e. magnetically inequivalent sites. One can roughly estimate that a  $\sim 35\%$  scatter of the projection of  $Mn^{2+}$  moment on the external field leads to the line broadening consistent with that observed in the experiment at 4 K (see Fig. 3).

In the well-known case of a commensurate Néel order, two magnetically inequivalent sites (magnetic sublattices) result in splitting of NMR peaks,<sup>18</sup> while in the current study a broader peak is observed instead, Fig. 3. Therefore, the  $Mn^{2+}$  spins in this system freeze below  $T_{MI}$  into a more intricate magnetic state or an incommensurate long-range order. This is probably because manganese forms a nearly triangular network in the anion layer. In such systems with AF coupling where the minimization of pairwise interactions is geometrically frustrated, exotic magnetic structures are often resolved in the ground state.<sup>19</sup>

### C. Magnetic torque

The magnetic torque defined as  $\vec{\tau} = \vec{M} \times \vec{H}$ , was measured in field sweeps between 0 and 150 kOe. The field orientation with respect to the  $a^*$  direction, determined by polar angle  $\beta$ , was spanned around four directions included in the ( $bc$ )-plane:  $b$ -axis,  $c$ -axis,  $[0\bar{1}1]$  direction, and the direction perpendicular to  $[0\bar{1}1]$ . The experimental geometry for the  $c$ -axis rotation is illustrated in the bottom left of Figure 4. The torque meter is constructed to pick up the torque component along the rotation axis because its cantilever is mounted perpendicular to the goniometer axis.

The left panel in Figure 4 shows several  $c$ -axis torque curves measured at 1.4 K. One can see that the main contribution to the torque monotonically develops with the field and saturates above 100 kOe. The flattening

of the torque results apparently from the competition between the magnetic energy, which forces the saturated magnetic moment to align with the field direction, and the magnetic anisotropy, which tends to bring it along the axis of easy magnetization. Such behavior of the torque at high fields/low temperatures was observed, for instance, in  $\lambda$  and  $\kappa$  phases of  $(\text{BETS})_2\text{FeCl}_4$ .<sup>20,21</sup>

The behavior of the monotonic contribution to the torque has a  $\sin 2\beta$  periodicity and is qualitatively the same for all four directions of the rotation axis. The angular dependences of the torque at  $T = 1.4\text{ K}$ ,  $H = 150\text{ kOe}$  fit the relation  $\tau(\beta) = A \sin 2(\beta - \beta_0)$  with parameters  $A$  and  $\beta_0$  listed in Table I.

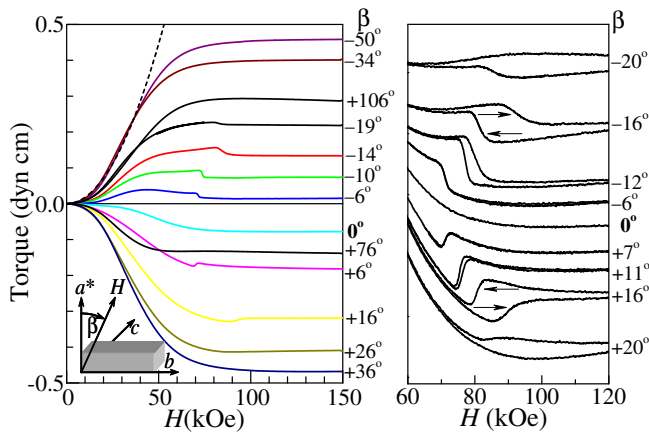


FIG. 4: Left panel: Field dependences of the  $c$ -axis torque at 1.4 K at different angles. Dashed line:  $\frac{1}{2}\Delta\chi H^2$  with  $\Delta\chi = 0.012\text{ cm}^3/\text{mol}$ , see text. Bottom left diagram: experimental geometry. Right panel: The region with the kinks close-up. The curves are offset along the vertical axis for better visualization. Arrows indicate the field sweep directions. Numbers to the right of each panel indicate the angle between the field direction and the  $a^*$ -axis.

TABLE I: Parameters of the torque angular dependence at  $T = 1.4\text{ K}$ ,  $H = 150\text{ kOe}$ .  $\beta$  is the angle between the field direction and  $a^*$ .

Rotation axis	$\tau(\beta) = A \sin 2(\beta - \beta_0)$	
	$A$	$\beta_0(\pm 1^\circ)$
$\parallel [0\bar{1}0]$ ( $b$ -axis)	3.5	$-69^\circ$
$\parallel [001]$ ( $c$ -axis)	0.92	$85^\circ$
$\parallel [0\bar{1}1]$	2.1	$-66^\circ$
$\perp [0\bar{1}1]$ within $(bc)$ plane	2.8	$67^\circ$

In order to understand the extent of the magnetic anisotropy given by the measured torque, an estimate calibration of the torque meter was done using the cantilever geometry and the Young's modulus of its material. Calculations give a factor  $\sim 0.5\text{ dyn-cm/unit}$  for the vertical scale in Fig. 4 and for the  $A$  parameter in Table I.

As one can see in Fig. 4, at low fields the torque is approximately quadratic in field. This behavior expressed

as  $\tau = \frac{1}{2}\Delta\chi H^2 \sin 2(\beta + \beta_0)$  can be used to estimate the susceptibility anisotropy,  $\Delta\chi$ , in the plane normal to the rotation axis. Using the above calibration factor, one obtains  $\Delta\chi_{a^*b} \simeq 0.012\text{ cm}^3/\text{mol}$  for the  $c$ -axis torque. In a similar way, for the  $b$ -axis torque our data gives  $\Delta\chi_{a^*c} \simeq 0.03\text{ cm}^3/\text{mol}$ . The anisotropy is therefore  $\leq 5\%$  of the susceptibility ( $0.66\text{ cm}^3/\text{mol}$  at 2 K), which appears negligibly small in the dc magnetization measurements presented above. However, these values are at least an order of magnitude bigger compared to organic compounds with non-magnetic anion layers.<sup>18,22</sup> Therefore the dominating contribution to the torque comes from the anisotropy in the  $\text{Mn}^{2+}$  magnetic subsystem. Importantly, none of the principal axes of this magnetic subsystem coincide with the crystallographic axes (see Table I) because the torque along a principal magnetic axis is identically zero. Moreover, well above the MI transition the torque still zeroes at angles close to  $\beta_0$  which means that the orientation of the principal axes of  $\text{Mn}^{2+}$  subsystem does not change appreciably at  $T_{MI}$ .

It should be mentioned that while the high-field torque zeroes at angles  $\beta = \beta_0$  and  $\beta_0 \pm \pi/2$ , at low temperature the low-field torque ( $H < 50\text{ kOe}$ ) for these directions does not vanish completely showing a small bell-like feature, as has also been noticed in Ref. 10. The origin of this feature is so far unclear and requires further investigation. Anyway, the periodicity of this feature is a regular  $\sin 2\beta$ . Therefore, it cannot be ascribed to a conventional spin-flop transition in a uniaxial antiferromagnet, which is periodic as  $\text{sgn}\beta \cos \beta$ .<sup>23</sup>

As one can see in Fig. 4, at small angles  $\beta$  the monotonic development of the torque is broken by a step-like feature, or a ‘‘kink’’. A similar behavior, though with somewhat smaller kinks, has also been found for the field rotations around  $[0\bar{1}1]$  and around the axis perpendicular to  $[0\bar{1}1]$ , whereas no kinks have been detected in the  $b$ -axis torque curves.

The angular evolution of the kink is shown in more detail in the right panel in Fig. 4. The behavior of the kink with the field and the angle is quite peculiar. First, it emerges in a rather symmetric way with tilting the field from  $H \parallel a^*$  ( $\beta = 0$  and  $\pm\pi$ ) and is not seen around  $H \perp a^*$  ( $\beta = \pm\pi/2$ ): compare curves for  $\beta = -14^\circ$  and  $+76^\circ$ , and for  $\beta = +16^\circ$  and  $+106^\circ$  in the right panel in Fig. 4. The kink periodicity is therefore  $\text{sgn}\beta \cos \beta$ , which is the same as for the torque at the spin-flop transition. Secondly, the kink moves up in field with increasing the tilt from the  $a^*$  direction, and vanishes when the tilt is more than  $20^\circ$ , which means that we deal with a projection of some preferential direction on  $a^*$ . Thirdly, it becomes increasingly hysteretic at  $\beta > \pm 10^\circ$  indicating a first-order transition. With increasing temperature, the kink becomes smaller and disappears above 25 K, as illustrated in Figure 5 where the  $c$ -axis torque field derivative,  $d\tau/dH$ , for  $\beta = +10^\circ$  is plotted for temperatures from 1.4 to 25 K. The inset in Fig. 5 shows temperature dependence of the  $d\tau/dH$  peak height. The listed peculiarities of the kink behavior in the insulating state indicate an

abrupt field-induced reorientation of magnetic moments, quite reminiscent of a spin-flop transition in an antiferromagnet.

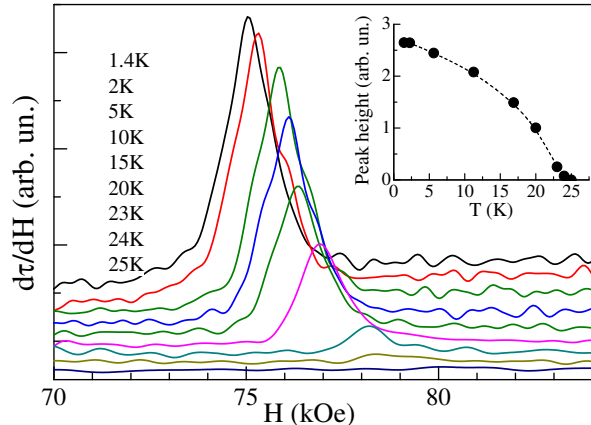


FIG. 5: (Color online) The field derivative of the torque,  $d\tau/dH$ , as a function of field for  $\beta = +10^\circ$ , at temperatures from 1.4 K (the top curve) to 25 K (the bottom curve). Inset: Temperature dependence of the  $d\tau/dH$  peak height.

The direction  $a^*$  in which vicinity the spin-flop occurs should be close to the AF easy axis. As noted above, the  $a^*$  direction is not the principal axis of the magnetic subsystem associated with  $\text{Mn}^{2+}$  network. We therefore speculate that the kink is related to another magnetic subsystem, namely to localized  $\pi$ -electron spins in BETS layers. Indeed, if the MI transition in the present compound is caused by the Mott instability,<sup>11</sup> one can expect the spins associated with the localized  $\pi$  electrons to be antiferromagnetically ordered. While we have currently no information about the principal axes of the  $\pi$ -electron spin system, it is likely that one of them is along  $a^* \perp bc$ , which is of course a special direction in this layered electronic system. The size of the kink,  $\sim 10$  times smaller than the maximum torque in Fig. 4, is also consistent with what one would expect as a contribution from  $\pi$  electrons on BETS molecules.<sup>18,22</sup>

There is a number of features that distinguish the observed field-induced transition from the usual spin-flop in a uniaxial antiferromagnet. In the latter case the spin-flop feature in the torque has a sharp  $\lambda$ -like shape. Such spin-flop transition occurs in  $\lambda\text{-(BETS)}_2\text{FeCl}_4$ <sup>24</sup> but at much lower field 12 kOe. However, in  $\lambda\text{-(BETS)}_2\text{FeCl}_4$  the  $\text{Fe}^{3+}$ -based anion subsystem is deeply involved into the formation of the AF order. This is inferred from the large drop of the static susceptibility<sup>12</sup> and the huge spin-flop feature in the torque<sup>24</sup> comparable with the maximum high-field torque. On the contrary, in the compound under study a long-range ordering in the  $\text{Mn}^{2+}$

magnetic subsystem is not as obvious. The geometrically frustrated Kagome-type lattice of  $\text{Mn}^{2+}$  is reluctant of Néel-type ordering, as can be concluded from the minor changes of the susceptibility (see Fig. 1). In turn, the frustrated  $\text{Mn}^{2+}$  subsystem can essentially modify the AF structure of the BETS  $\pi$ -electrons due to the  $\pi - d$  interactions.

#### IV. CONCLUSION

We have performed dc magnetization,  $^1\text{H}$  NMR and magnetic torque studies of organic conductor  $\kappa\text{-(BETS)}_2\text{Mn}[\text{N}(\text{CN})_2]_3$  which undergoes a MI transition at 25 K. The magnetization above  $T_{MI}$  follows the Curie-Weiss law, revealing antiferromagnetic interactions between  $S = 5/2$ ,  $L = 0$   $\text{Mn}^{2+}$  spins, and violates it at lower temperature. The  $^1\text{H}$  NMR spectrum determined by dipolar fields from  $\text{Mn}^{2+}$  moments, exhibits vast broadening of the resonance peaks below 25 K resulting from freezing of  $\text{Mn}^{2+}$  spins. Both the magnetization and NMR data obtained at fields below 70 kOe, therefore suggest a transition from paramagnetic to a frozen state in the manganese subsystem taking place at  $T_{MI}$ . However, the resulting state clearly differs from the conventional commensurate Néel type antiferromagnetic order.

Yet another signature of a magnetic transition is the kink in the field-dependent torque emerging right below  $T_{MI}$ . This one takes place above  $\sim 70$  kOe and possesses many properties of a spin-flop transition. Most likely it occurs within the spins of Mott-localized  $\pi$  electrons of BETS molecules. If so, it would be more natural to consider the Mott localization as a driving force for both the MI transition and magnetic transformations in the system. An additional argument towards this conclusion is a low  $\theta \sim -5$  K in the Curie-Weiss temperature dependence of the spin susceptibility (compared to  $T_{MI} \approx 25$  K): in a conventional antiferromagnet the AF transition usually occurs at temperature lower than  $|\theta|$ .<sup>25</sup> To further clarify this issue, NMR studies at higher fields where the kink appears would be very helpful.

#### V. ACKNOWLEDGEMENTS

This work was supported by the RFBR grants 07-02-91562, 10-02-01202 and DFG grant RUS 113/926/0. The authors gratefully acknowledge the assistance in the questions of crystallography from R. P. Shibaeva, S. S. Khasanov and S. V. Simonov and the technical support from N. A. Belov.

<sup>1</sup> T. Ishiguro, K. Yamaji, and G. Saito, *Organic superconductors* (Springer-Verlag, Berlin, 1988).

<sup>2</sup> *The Physics of Organic Superconductors and Conductors*, edited by A. G. Lebed (Springer Berlin Heidelberg, 2008).

- <sup>3</sup> E. Coronado and P. Day, *Chem. Rev.* **104**, 5419 (2004); T. Enoki and A. Miyazaki, *ibid.* **104**, 5449 (2004); H. Kobayashi, H. Cui, and A. Kobayashi, *ibid.* **104**, 5265 (2004).
- <sup>4</sup> L. Ouahab, in *Organic Conductors, Superconductors and Magnets: From Synthesis to Molecular Electronics* edited by L. Ouahab and E. Yagubskii (Kluwer Acad. Publ. Dordrecht/Boston/London, 2003), p. 99.
- <sup>5</sup> G. Saito and Y. Yoshida, *Bull. Chem. Soc. Jpn.* **80**, 1 (2007).
- <sup>6</sup> E. Coronado and K. R. Dunbar, *Inorg. Chem.* **48**, 3293 (2009).
- <sup>7</sup> L. Ouahab and T. Enoki, *Eur. J. Inorg. Chem.* **2004**, 933 (2004).
- <sup>8</sup> S. Uji, H. Shinagawa, T. Terashima, T. Yakabe, Y. Terai, M. Tokumoto, A. Kobayashi, H. Tanaka, and H. Kobayashi, *Nature* **410**, 908 (2001).
- <sup>9</sup> H. Fujiwara, H. Kobayashi, E. Fujiwara, and A. Kobayashi, *J. Am. Chem. Soc.* **124**, 6816 (2002).
- <sup>10</sup> N. D. Kushch, E. B. Yagubskii, M. V. Kartsovnik, L. I. Buravov, A. D. Dubrovskii, A. N. Chekhlov, and W. Biberacher, *J. Am. Chem. Soc.* **130**, 7238 (2008).
- <sup>11</sup> V. N. Zverev, M. V. Kartsovnik, W. Biberacher, S. S. Khasanov, R. P. Shibaeva, L. Ouahab, L. Toupet, N. D. Kushch, E. B. Yagubskii, and E. Canadell, *Phys. Rev. B* **82**, 155123 (2010).
- <sup>12</sup> L. Brossard *et al.*, *Eur. Phys. J. B* **1**, 439 (1998).
- <sup>13</sup> C. Hotta and H. Fukuyama, *J. Phys. Soc. Jpn.* **69**, 2577 (2000).
- <sup>14</sup> H. Akiba, S. Nakano, Y. Nishio, K. Kajita, B. Zhou, A. Kobayashi, and H. Kobayashi, *J. Phys. Soc. Japan* **78**, 033601 (2009).
- <sup>15</sup> J. C. Waerenborgh, S. Rabaça, M. Almeida, E. B. Lopes, A. Kobayashi, B. Zhou, and J. S. Brooks, *Phys. Rev. B* **81**, 060413(R) (2010).
- <sup>16</sup> P. Christ, W. Biberacher, H. Müller, K. Andres, *Solid State Commun.* **91**, 451 (1994).
- <sup>17</sup> For the field in the (*ac*) plane, every of the 8 hydrogen sites of the BETS molecule is mapped to a single line in NMR spectrum. However, a *b*-axis field component doubles the number of magnetically inequivalent hydrogen sites (hence the number of NMR peaks) due to the mirror-type ( $x, y, z$ )  $\rightarrow$  ( $x, -y, z$ ) symmetry operations of the space group  $P2_1/c$  (2-fold screw axis with direction [010] and glide plane normal to [010]).
- <sup>18</sup> K. Miyagawa, A. Kawamoto, Y. Nakazawa, and K. Kanoda, *Phys. Rev. Lett.* **75**, 1174 (1995).
- <sup>19</sup> S. T. Bramwell and M. J. P. Gingras, *Science* **294**, 1495 (2001).
- <sup>20</sup> T. Sasaki, H. Uozaki, S. Endo, and N. Toyota, *Synth. Metals* **120**, 759 (2001).
- <sup>21</sup> H. Uozaki, T. Sasaki, S. Endo, and N. Toyota, *J. Phys. Soc. Jpn.* **69**, 2759 (2000).
- <sup>22</sup> W. Biberacher, P. Christ, M. V. Kartsovnik, D. Andres, H. Müller, and N. Kushch, *J. Phys. IV France* **114**, 291 (2004).
- <sup>23</sup> K. Yoshida, *Prog. Theor. Phys.* **6**, 691 (1951).
- <sup>24</sup> M. Tokumoto, H. Tanaka, T. Otsuka, H. Kobayashi, and A. Kobayashi, *Polyhedron* **24**, 2793 (2005).
- <sup>25</sup> A. H. Morrish, *The Physical Principles of Magnetism* (Wiley-IEEE Press, New York, 2001).